

Identification of cathode materials for lithium batteries guided by first-principles calculations

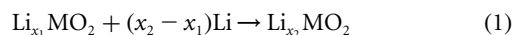
G. Ceder, Y.-M. Chiang, D. R. Sadoway, M. K. Aydinol, Y.-I. Jang & B. Huang

Department of Materials Science and Engineering, Massachusetts Institute of Technology, Cambridge, Massachusetts 02139-4307, USA

Lithium batteries have the highest energy density of all rechargeable batteries and are favoured in applications where low weight or small volume are desired—for example, laptop computers, cellular telephones and electric vehicles¹. One of the limitations of present commercial lithium batteries is the high cost of the LiCoO₂ cathode material. Searches for a replacement material that, like LiCoO₂, intercalates lithium ions reversibly have covered most of the known lithium/transition-metal oxides, but the number of possible mixtures of these^{2–5} is almost limitless, making an empirical search labourious and expensive. Here we show that first-principles calculations can instead direct the search for possible cathode materials. Through such calculations we identify a large class of new candidate materials in which non-transition metals are substituted for transition metals. The replacement with non-transition metals is driven by the realization that oxygen, rather than transition-metal ions, function as the electron acceptor upon insertion of Li. For one such material, Li(Co,Al)O₂, we predict and verify experimentally that aluminium substitution raises the cell voltage while decreasing both the density of the material and its cost.

The important characteristics of a lithium/metal-oxide compound for battery applications include the voltage at which it exchanges lithium, the amount of lithium that can be reversibly intercalated, and the stability of the material. The first two properties determine the energy density, and the latter limits the lifetime of the battery. Although a high voltage is desirable for obtaining high energy density³, the practical use of high-voltage cathodes is at present limited by the voltage range over which the electrolyte is stable. The recent development of high-voltage electrolytes⁶ is, however, likely to ameliorate this problem.

We demonstrated recently^{7,8} that the average potential for intercalation between two compositions x_1 and x_2 can be obtained from the energy change in the reaction:



The advantage of a first-principles computation is that it can be used to calculate the energy of the three compounds in equation (1), and hence the average potential, for any metal M (or combination of them), in any structure, whether these conditions have been experimentally realized or not. To calculate the total energies in equation (1) we use the *ab initio* ultrasoft-pseudopotential method as implemented in ref. 9. For the reactions $\text{Li} + \text{Mn}_2\text{O}_4 \rightarrow \text{LiMn}_2\text{O}_4$ and $\text{Li} + \text{CoO}_2 \rightarrow \text{LiCoO}_2$ we find average potentials of 4.0 and 3.75 V, respectively. The measured values are approximately 4.1 and 4.0 V, indicating that we have reasonable agreement with experiment, even though there are no adjustable parameters in the theory. The errors are consistent with the systematic underprediction of the potential in these compounds by ~ 0.2 V (ref. 7). Clearly, the *ab initio* prediction of intercalation voltages is possible. New materials can therefore be pre-screened before attempting their synthesis.

It is traditionally assumed that the intercalation voltage is determined by the redox potential of the transition-metal ion

which is believed to change valence on Li insertion. We recently argued that for the late-transition-metal oxides it is instead the oxygen which is in large part responsible for the electron exchange⁷. As electron exchange with oxygen leads to a lower electrostatic energy (hence a higher voltage), we speculated that increased voltage correlates with increased oxygen participation in the electron exchange. If this is correct, part or all of the transition metal in a cathode material could be replaced by non-transition-metal ions, while retaining electrochemical Li-activity, although at a higher voltage. Such substitution would significantly increase the number of compounds that can be considered as cathode-active materials. In particular, elements from the third row of the periodic table would be of interest as they have lower mass than the 3*d* metals.

In this work, we first calculated the hypothetical intercalation voltage in Li_{*x*}AlO₂ and found it to be 5.4 V. LiAlO₂ has empty Al *p* orbitals well above the filled oxygen *p* states with no *d* states in between (as have all the transition-metal oxides) and electron exchange therefore occurs completely with the oxygen bands. Experimentally, this Li intercalation capacity will probably not be accessible as LiAlO₂ is electronically insulating. Electronic conductivity is required in an intercalation oxide, as Li⁺ diffusion can occur only when accompanying electron motion is also possible. However, in solid solution with other transition-metal oxides, LiAlO₂ may be an attractive component. If our prediction regarding electrochemical activity of the oxygen ion is correct, Al substitution for transition-metal oxides will lead to higher Li intercalation voltage, as the fixed 3+ valence of Al forces more electron exchange with oxygen. However, our calculations indicate potential difficulties for mixing LiAlO₂ with other lithium/metal-oxides. We calculated the formation enthalpy for Li(M,Al)O₂ mixtures with M = Ti, V, Fe, Co and found them all to be positive, indicating that, at least at low temperature, separate regions of LiAlO₂ and LiMO₂ are favoured over the solid solution. Only in Li(Co,Al)O₂ is the formation enthalpy small enough (30 meV) to allow for entropy-driven mixing. We note that previous investigations of Al-doping of transition-metal oxides show no apparent effect on the intercalation potential^{10,11}. However, phase separation at a scale not detectable by X-rays would annihilate the effect of Al doping on the potential, and result in a material with properties indistinguishable from the undoped material.

For Li(Al_{0.33}Co_{0.67})O₂ and Li(Al_{0.67}Co_{0.33})O₂ in the α -NaFeO₂ structure, our first-principles calculations predict an average Li intercalation potential of respectively 4.2 and 4.7 V. Given the

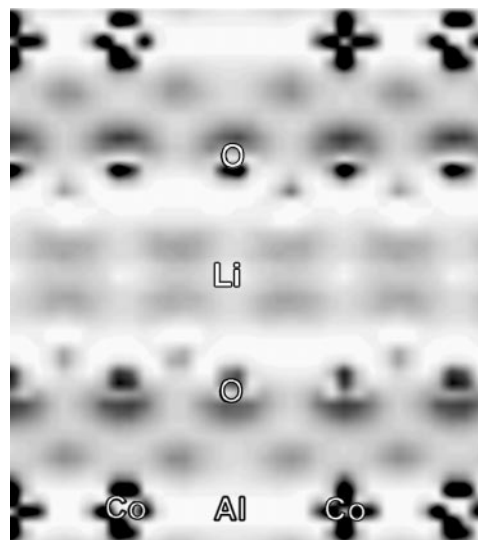


Figure 1 Positive part of the electron density difference between Li(Al_{0.33}Co_{0.67})O₂ and (Al_{0.33}Co_{0.67})O₂ in a plane perpendicular to the direction of layering in the structure. Darker indicates larger electron density.

consistent underestimation of experimental voltages by the calculations⁷, the true potential is probably ~0.2 V higher. The increase in voltage over pure LiCoO₂ is in agreement with our understanding of the increasing role of oxygen in Al-doped material. Figure 1 shows the change in charge density of the valence electrons when going from (Al_{0.33}Co_{0.67})O₂ to Li(Al_{0.33}Co_{0.67})O₂. These results are obtained by subtracting the charge density in (Al_{0.33}Co_{0.67})O₂ from that in Li(Al_{0.33}Co_{0.67})O₂. For these calculations, all atomic positions were assumed to remain unchanged on lithiation (whereas all coordinates were fully relaxed for the voltage calculations). Although Co accepts some charge from the extra lithium atom, none is transferred to Al. Considerable charge transfer to oxygen is clearly visible.

To test the predictions of the computations we developed a method to synthesize homogeneous Li(Co,Al)O₂ solid solutions in the α-NaFeO₂ structure. First, mixed cobalt–aluminium hydroxides were precipitated from mixed aqueous solutions containing Co(NO₃)₂ and Al(NO₃)₃, added dropwise to a continuously stirred LiOH aqueous solution kept at pH 10.5. Nitrate ions were removed from the precipitate through a rinsing procedure described in ref. 12. Lithium was then added through a freeze-drying procedure, in which the mixed hydroxide was dispersed in aqueous LiOH solution yielding a total Li/(Co + Al) molar ratio of unity, the suspension was atomized into liquid nitrogen, and the frozen droplets were freeze-dried.

Transmission electron microscopy showed this precursor to consist of crystalline Co,Al hydroxide uniformly mixed with amorphous Li hydroxide at the submicrometre scale. X-ray powder diffraction showed that a single-phase solid solution in the α-NaFeO₂ structure (space group *R*3̄*m*) is obtained on firing this precursor to *T* > 400 °C in air for the compositions *y* = 0.25 and *y* = 0.5. For *y* = 0.75, a two-phase mixture of the α-NaFeO₂ solid solution and the tetragonal phase of LiAlO₂ was obtained.

Cathodes containing LiAl_{*y*}Co_{1-*y*}O₂ were prepared by mixing the oxide powder with carbon black and potting the mixture in a binder of poly(vinylidene fluoride). Pellets weighing 10–35 mg and measuring 1.0 cm² in surface area were formed by pressing at 360 MPa. These were dried at 140 °C under primary vacuum for 24 h and transferred to an argon-filled glove box. The test cell consisted of two stainless-steel electrodes in a holder made of Teflon. The anode was a lithium ribbon 0.75 mm thick. The electrolyte consisted of a 1 M solution of LiPF₆ in ethylene carbonate–diethyl carbonate, 1:1 by volume. The separator was a film of Celgard 2400 (Celgard LLC,

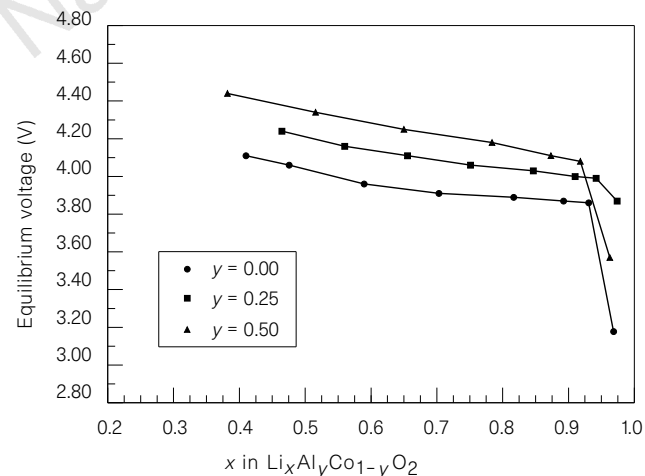


Figure 2 Open-circuit potential as a function of lithium content in pure LiCoO₂ and in Al-doped materials.

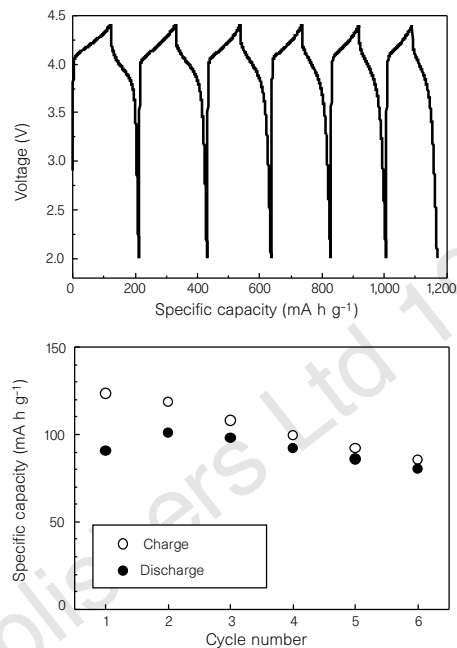


Figure 3 Cycling behaviour of Li(Al_{0.25}Co_{0.75})O₂/Li and specific capacity between 2.0 and 4.4 V. The current density was 0.4 mA cm⁻².

Charlotte, North Carolina). Charge/discharge tests were performed with a Maccor Series 4000 Automated Test System (Maccor Inc., Tulsa, Oklahoma).

Figure 2 shows the open-circuit voltage (equilibrium potential) as a function of Li content in the oxide for samples calcined at 850 °C. These results were obtained by charging the cell in steps and allowing it to equilibrate for 15 h after each step. The equilibrium potential of the cells increases systematically with the Al content in the oxide, confirming the theoretical predictions. We note that at a value of 1 - *x* = 0.4 the equilibrium voltage of the Li_{1-*x*}Al_{0.5}Co_{0.5}O₂/Li cell was as high as 4.40 V. As the calculations give the average voltage between compositions MO₂ and LiMO₂, whereas the cells were charged over only part of this composition range, direct quantitative comparison of the theoretical and experimental voltage is not yet possible.

Figure 3 shows the first few charges and discharges between 2.0 and 4.4 V (current density of 0.4 mA cm⁻²) for the LiAl_{0.25}Co_{0.75}O₂/Li cell. The initial charge and discharge capacity were 120 and 90 mA h g⁻¹, respectively. On the sixth cycle, charge and discharge in the same potential window resulted in a capacity of ~90 and 80 mA h g⁻¹, respectively. The 4.4 V charging limit is imposed by the stability of the electrolyte used in these experiments and it is likely that more capacity could be found at higher potentials. The material clearly shows some capacity fade, as has been the case with many Li insertion materials in the initial stage of their development.

We expect similar results to these in other LiAl_{*y*}M_{1-*y*}O₂ solid solutions, where M is a transition metal. The present results show that the intercalation potential of such solid solutions, and probably those of other structures such as the spinel, can be 'quantum-engineered'. Owing to its low weight and price, aluminium can significantly increase energy density while reducing cost. Commercial feasibility of any new material will, however, also rely on successful synthesis and demonstration of high capacity and stability under electrochemical cycling. □

Received 20 August 1997; accepted 9 February 1998.

1. Pistoia, G. *Lithium Batteries* (Elsevier, Amsterdam, 1994).
2. Delmas, C. & Saadoun, I. Electrochemical and physical properties of the Li_{1-*x*}Ni_{*y*}Co_{*z*}O₂ phases. *Solid State Ionics* **53–56**, 370–375 (1992).
3. Fey, G., Li, W. & Dahn, J. R. LiNiVO₄: A 4.8 Volt electrode material for lithium cells. *J. Electrochem. Soc.* **141**, 2279–2282 (1994).
4. Reimers, J. N., Rosen, E., Jones, C. D. & Dahn, J. R. Structure and electrochemistry of Li_{1-*y*}Fe_{*y*}Ni_{1-*y*}. *Solid*

State Ionics 61, 335–334 (1993).

5. Ohzuku, T., Ueda, A., Nagayama, M., Iwakoshi, Y. & Komori, H. Comparative study of LiCoO₂, LiNi_{1/2}Co_{1/2}O₂ and LiNiO₂ for 4 volt secondary lithium cells. *Electrochim. Acta* 38, 1159–1167 (1993).
6. Tarascon, J. M. & Guyomard, D. New electrolyte compositions stable over the 0 to 5 V voltage range and compatible with the Li_{1+x}Mn₂O₄/carbon Li-ion cells. *Solid State Ionics* 69, 293–305 (1994).
7. Aydinol, M. K., Kohan, A. F., Ceder, G., Cho, K. & Joannopoulos, J. Ab-initio study of lithium-intercalation in metal-oxides and metal-dichalcogenides. *Phys. Rev. B* 56, 1354–1365 (1997).
8. Ceder, G., Aydinol, M. K. & Kohan, A. F. Application of first-principles calculations to the design of rechargeable Li-batteries. *Comput. Mater. Sci.* 8, 161–169 (1996).
9. Kresse, G. & Furthmüller, J. Efficiency of ab-initio total energy calculations for metals and semiconductors using a plane-wave basis set. *Comput. Mater. Sci.* 6, 15–50 (1996).
10. Nazri, G. A., Rougier, A. & Kia, K. F. in *Solid State Chemistry of Inorganic Materials* (eds Davies, P. K., Jacobson, A. J., Torardi, C. C. and Vanderah, T. A.) 635–646 (Mater. Res. Soc. Symp. Proc. 453, Materials Research Society, Pittsburgh, 1997).
11. Ohzuku, T., Ueda, A. & Kouguchi, M. Synthesis and characterization of LiAl_{1/3}Ni_{3/4}O₂(R3m) for lithium-ion (shuttlecock) batteries. *J. Electrochem. Soc.* 142, 4033–4039 (1995).
12. Chiang, Y.-M. *et al.* Synthesis of LiCoO₂ by decomposition and intercalation of hydroxides. *J. Electrochem. Soc.* 145, 887–891 (1998).

Acknowledgements. We thank A. Mays for discussions and comments. This work was sponsored by Furukawa Electric and the US Department of Energy through the Idaho National Engineering Laboratory University Research Consortium.

Correspondence and requests for materials should be addressed to G.C. (e-mail: gerd@lanai-mit.edu).

Surface topography dependence of biomolecular hydrophobic hydration

Yuen-Kit Cheng & Peter J. Rossky

Department of Chemistry and Biochemistry, University of Texas at Austin, Austin, Texas 78712-1167, USA

Many biomolecules are characterized by surfaces containing extended nonpolar regions¹, and the aggregation and subsequent removal of such surfaces from water is believed to play a critical role in the biomolecular assembly in cells². A better understanding of the hydrophobic hydration of biomolecules may therefore yield new insights into intracellular assembly. Conventional views hold that the hydration shell of small hydrophobic solutes is clathrate-like, characterized by local cage-like hydrogen-bonding structures and a distinct loss in entropy². The hydration of extended nonpolar planar surfaces, however, appears to involve structures that are orientationally inverted relative to clathrate-like hydration shells^{3,4}, with unsatisfied hydrogen bonds that are directed towards the hydrophobic surface. Here we present computer simulations of the interaction between the polypeptide melittin and water that demonstrate that the two different hydration structures also exist near a biomolecular surface. We find that the two structures are distinguished by a substantial difference in the water–water interaction enthalpy, and that their relative contributions depend strongly on the surface topography of the melittin molecule: clathrate-like structures dominate near convex surface patches, whereas the hydration shell near flat surfaces fluctuates between clathrate-like and less-ordered or inverted structures. The strong influence of surface topography on the structure and free energy of hydrophobic hydration is likely to hold in general, and will be particularly important for the many biomolecules whose surfaces contain convex patches, deep or shallow concave grooves and roughly planar areas⁵.

The magnitude of the free energy of hydrophobic hydration, as inferred from the solubilities of small hydrocarbons in water, is ~25 cal mol⁻¹ Å⁻² and is typically assumed to depend predominantly on the solute surface area⁶. This, and similar values derived from the data⁶, are relatively low when compared with (for instance) the corresponding macroscopic measure of the liquid pentane–water interface, which is ~72 cal mol⁻¹ Å⁻². Although the origin of this large difference remains controversial (see ref. 7 for a review), it is reasonable to anticipate that the molecularity of the solvent and solute are relevant to the value obtained.

Amphipathic helical polypeptides (with segregation of hydrophilic and hydrophobic moieties) have been chosen as the target in this study. Melittin, a 26-mer polypeptide found in honeybee venom, is one of the most studied archetypes of membrane proteins⁸. It readily self-associates as a tetramer in an aqueous solution of high peptide concentration, high pH, or high ionic strength⁸. Crystallized as a tetramer, it is spatially a dimer of two almost stereochemically identical amphipathic α-helical dimers related by a two-fold symmetry axis⁹. Each dimer possesses a relatively flat hydrophobic surface, surrounded by convex patches of hydrophobic moieties (Fig. 1); the flat surface is completely buried in the centre of the tetramer on tetramerization⁹. Self-association of α-helical melittin monomers is thought to be important in its lytic activity of membranes, although the actual mechanism is still unknown. (See ref. 8 for a review.)

The interfacial hydration properties are expected to be crucial to the role of hydrophobic hydration of membrane proteins preceding and during membrane association. As the hydration of extended hydrophobic surfaces is apparently common in biological processes (for example, as inferred in the functioning surfaces of chaperonins¹⁰), results regarding hydrophobic hydration of surfaces, explored in this study, are of significance to a wider range of processes and compounds than the mechanism of melittin in membrane lysis.

In the following analysis, the surface of a melittin dimer is partitioned into two main types, ‘flat’ and ‘convex’, according to the local surface curvature (see Fig. 1). The coordinates of the dimer were extracted from the crystal structure of melittin tetramer⁹ deposited in the Brookhaven Protein Data Bank¹¹ and its structure was kept rigid throughout the simulation. The use of a fixed protein structure is not implemented as a simplification, but rather is required if one is to specifically identify the nature of hydration that is compatible with a given geometry of the protein surface. It is of interest also to learn how this protein structure might relax in response to full solvent exposure, but the present approach is needed if one is to understand the physical reasons for that process. Studies on the dynamics and other aspects of monomeric melittin in solution can be found elsewhere¹². The present simulation (see Methods section) was performed at a temperature of 300 K in the

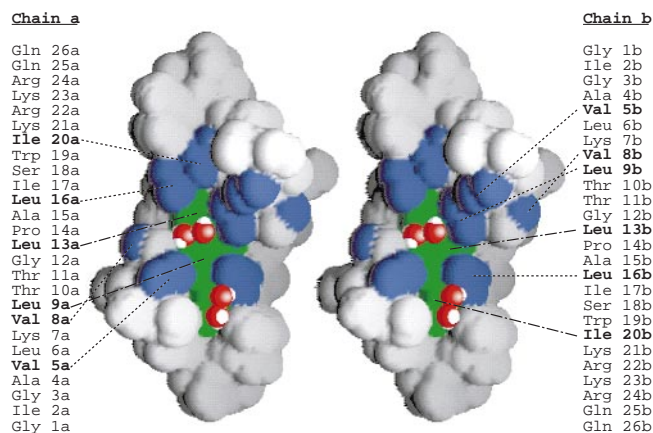


Figure 1 Stereographic image of the hydrophobic surface of the melittin dimer⁹; this is completely buried on tetramerization. The peptide sequences are provided in standard notation and are aligned with the model; the surface carbon centres selected for hydration analysis are indicated in bold. The central contiguous segment (shown green) is relatively flat and long (accessible surface area, 72.4 Å²); the small convex surface patches are shown blue. Four surface proximal water molecules (rendered with oxygen radius $r_{\text{wo}} = 1.6$ Å and hydrogen radius $r_{\text{wh}} = 1.0$ Å; oxygen atoms are shown in red) are overlaid on the images. Surface regions not considered in this analysis are shown white. The picture is rendered by the program GRASP²², and accessible surface area calculations by GEPOL93¹⁶.